Electronic Supplementary Material (ESI) for Journal of Materials Chemistry C.

SUPPORTING INFORMATION

Competitive electronic and steric effects in spin-state modulation of a 3D-Hofmann framework and its extension toward nanoscale

Dibya Jyoti Mondal, Bhart Kumar, Abhik Paul, Sanjit Konar *

Molecular Magnetism Lab, Department of Chemistry
Indian Institute of Science Education and Research
Bhopal Madhya Pradesh, India 462066
E-mail: skonar@iiserb.ac.in

Physical Measurement:

Fourier Transform Infrared Spectroscopy. The FT-IR experiment of microcrystalline bulk samples (1, 2 and 3) and nanoparticles (**NP1, NP2** and **NP3**) were recorded in transmittance mode using a Perkin Elmer spectrometer and attenuated total reflection (ATR) correction setup has been done between the range of 400–4000 cm^{-1}. To guarantee optimal optical contact, the powdered samples were squeezed between a diamond crystal and a bridge clamped sapphire anvil. the peaks were assigned based on the reported literature.

Thermogravimetric Analysis. The thermal stability of the samples was analyzed with a Perkin Elmer TGA-6000 thermobalance operating at a heating rate of 10 K min^{-1}, under anaerobic conditions (dry N2 atmosphere).

Powder XRD. Powder X-Ray Diffraction Patterns of all the crystals were obtained at 298 K on PANalytical Empyrean X-Ray Diffractometer with a Cu Kα radiation (λ=1.54060Å). The bulk powder of each sample was placed on a silica sample holder and measured by a continuous scan between 5–60º with a step size of 0.013103˚.

Single Crystal X-ray Diffraction (SCXRD) Single Crystal X-ray Diffraction data were collected on Bruker D8 Venture diffractometer using monochromated Mo Kα radiation (λ = 0.71073 Å) at 100 K using an Oxford Cryostream low-temperature device and also at 300 K temperatures. Unit cell measurements, data integration, scaling and absorption corrections for the crystals were done with Bruker APEX-3 software. Data reduction was carried out with Bruker SAINT suite. Absorption correction was performed by multi-scan method implemented in SADABS. All the crystal structures were solved by direct methods using SIR 2014. The crystal structure refinements were done in the program package *Olex2*,[1] and all non-hydrogen atoms were refined anisotropically by full matrix least-squares calculations based on F2 with SHELXL-2018.[2] Some hydrogen atoms were located from the difference Fourier Map, while the remaining hydrogen atoms were included in calculated positions as riding atoms. Details of crystal data, data collection, and refinement details are given in Table S1. The distortion parameters (Σ) were calculated using the OctaDist tool.[3]

Magnetic Susceptibility Measurements. Magnetic measurements were performed by using a Quantum Design MPMS2 SQUID magnetometer equipped with a 7 T magnet, operating at 1 T and at temperatures 2−400 K. The measured values were corrected for the experimentally measured contribution of the sample holder, whereas the derived susceptibilities were corrected for the diamagnetic contribution of the sample, estimated from Pascal's tables.

Scanning Electron Microscopy. The particle size of the nanoparticle and polymer samples were investigated using Carl Zeiss (Ultraplus) FESEM, FEI TALOS 200S HRTEM, and Agilent 5500 AFM/SPM instruments.

Table S1. Crystal data and structure refinement for complex **1.**

Empirical formula	$C_{33}H_{18}Fe_2N_{15}O_2Pd_2$
Formula weight	981.12
Temperature/K	100.0
Crystal system	orthorhombic
Space group	*Pbam*
a/Å	13.893(3)
b/Å	26.578(5)
c/Å	7.1985(13)
α/°	90
β/°	90
γ/°	90
Volume/Å3	2658.1(9)
Z	2
ρcalcg/cm3	1.226
μ/mm-1	1.238
F(000)	962.0
Crystal size/mm3	0.15 × 0.12 × 0.08
Radiation	MoKα (λ = 0.71073)
2Θ range for data collection/°	5.454 to 52.322
Index ranges	-15 ≤ h ≤ 17, -32 ≤ k ≤ 32, -8 ≤ l ≤ 8
Reflections collected	35303
Independent reflections	2799 [Rint = 0.1245, Rsigma = 0.0551]
Data/restraints/parameters	2799/0/143
Goodness-of-fit on F2	1.110
Final R indexes [I>=2σ (I)]	R1 = 0.0772, wR2 = 0.1971
Final R indexes [all data]	R1 = 0.0853, wR2 = 0.2019
Largest diff. peak/hole / e Å-3	2.74/-4.92

Table S2. Crystal data and structure refinement for complex **2.**

Empirical formula	$C_{44}H_{38}Fe_2N_{14}O_8Pd_2$	$C_{44}H_{38}Fe_2N_{14}O_8Pd_2$
Formula weight	1215.32	1215.32
Temperature/K	100.0	240.0
Crystal system	orthorhombic	orthorhombic
Space group	*Pbam*	*Pbam*
a/Å	13.5902(16)	13.4630(9)
b/Å	26.499(3)	27.3413(17)
c/Å	7.2586(9)	7.4818(4)
α/°	90	90
β/°	90	90
γ/°	90	90
Volume/Å^3	2614.0(5)	2754.0(3)
Z	2	2
ρ_{calc}g/cm^3	1.534	1.456
μ/mm^{-1}	1.282	1.217
F(000)	1200.0	1200.0
Crystal size/mm^3	0.16 × 0.1 × 0.08	0.16 × 0.1 × 0.08
Radiation	MoKα (λ = 0.71073)	MoKα (λ = 0.71073)
2Θ range for data collection/°	5.5 to 49.514	5.398 to 50.038
Index ranges	-15 ≤ h ≤ 15, -31 ≤ k ≤ 31, -8 ≤ l ≤ 8	-16 ≤ h ≤ 16, -32 ≤ k ≤ 32, -8 ≤ l ≤ 8
Reflections collected	37698	40938
Independent reflections	2426 [R_{int} = 0.1000, R_{sigma} = 0.0377]	2617 [R_{int} = 0.0664, R_{sigma} = 0.0265]
Data/restraints/parameters	2426/0/176	2617/0/170
Goodness-of-fit on F^2	1.080	1.127
Final R indexes [I>=2σ (I)]	R_1 = 0.0752, wR_2 = 0.2117	R_1 = 0.0737, wR_2 = 0.2038
Final R indexes [all data]	R_1 = 0.0849, wR_2 = 0.2186	R_1 = 0.0802, wR_2 = 0.2090
Largest diff. peak/hole / e Å^{-3}	1.18/-2.53	2.92/-2.78

Table S3. Selected structural parameters for complex **1.**

Spin states	LS
Temperature	100 K
<Fe–N> [Å]	1.958
Σ [°] (Octahedral. Dist. Parameter)	14.254
Θ [°] (Trigonal. Dist. Parameter)	30.4429
ζ [Å] (Length. Dist. Parameter)	0.1457

Table S4. Selected structural parameters for complex **2**.

Spin states	LS	HS
Temperature	100 K	300 K
<Fe–N> [Å]	1.950	2.161
Σ [°] (Octahedral. Dist. Parameter)	15.569	16.969
Θ [°] (Trigonal. Dist. Parameter)	31.016	38.241
ζ [Å] (Length. Dist. Parameter)	0.148	0.126

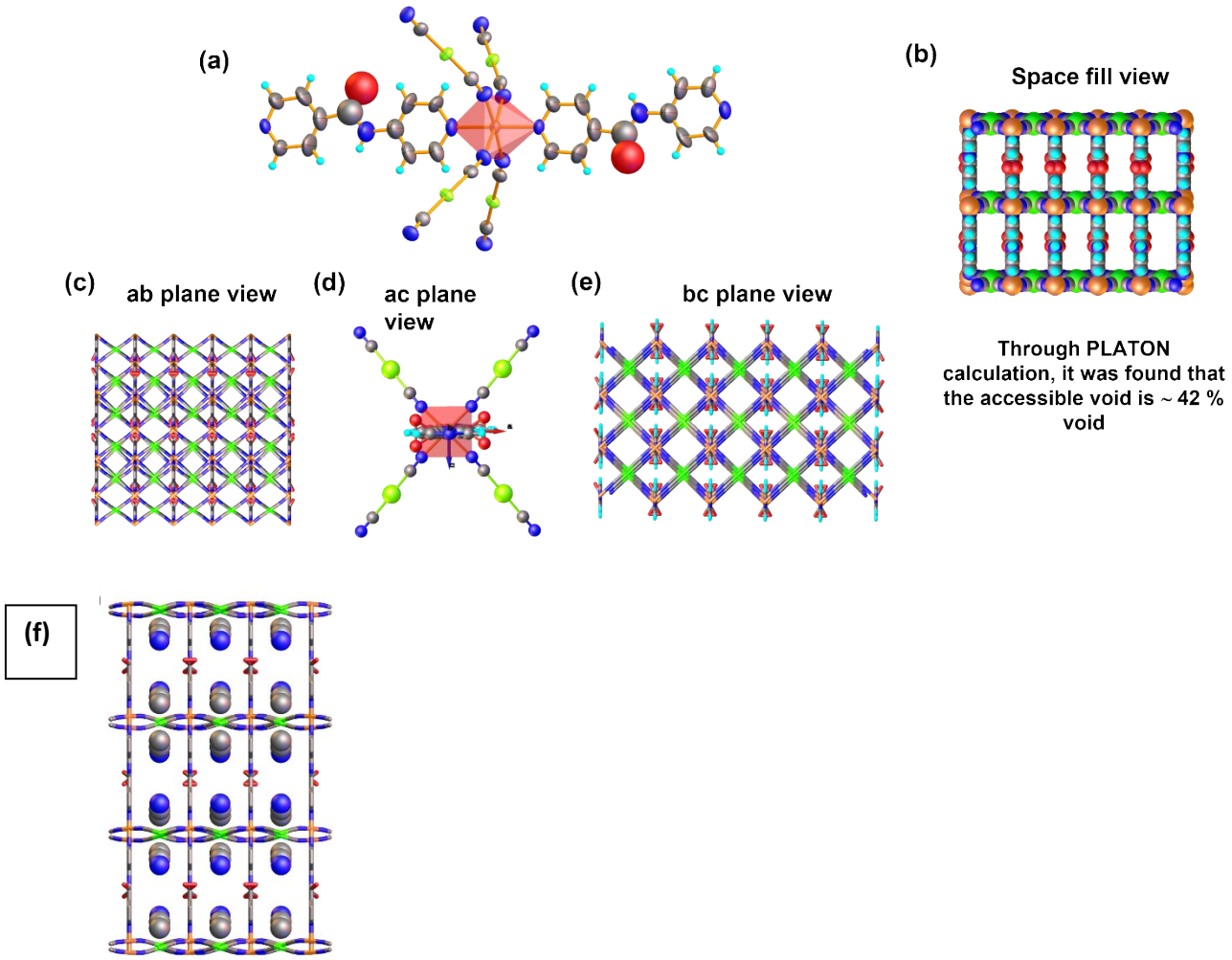

Figure S1. Structural parameters determined for complex **1** at 100 K. (a) octahedral coordination geometry around the SCO center; (b) space-filled model showing the solvent accessible void. (c-e) Representative view of the framework through crystallographic *c*, *b* and *a* axis respectively; (f) space-filled model of the acetonitrile molecules present in the pores of complex **1** viewed along plane 100.

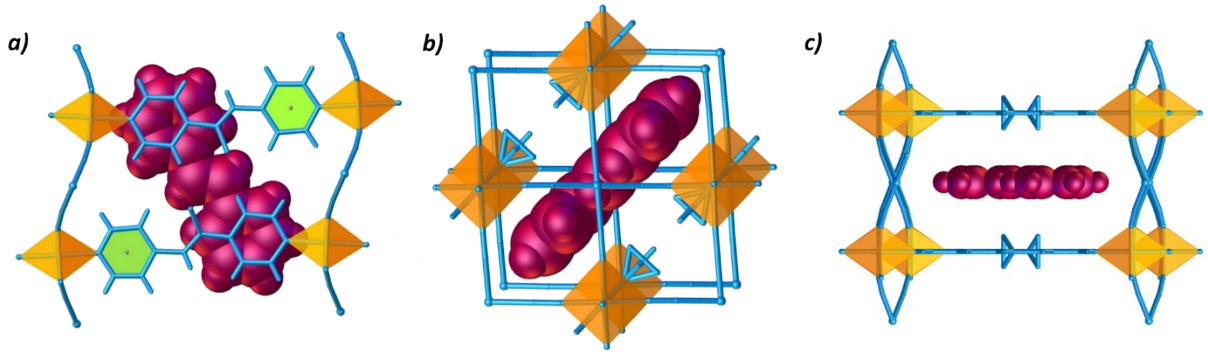

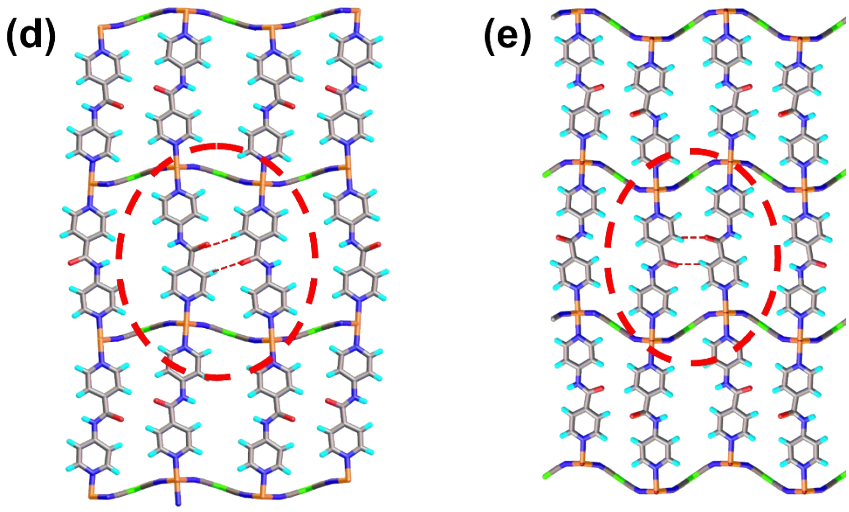

Figure S2. Representative stilbene filled host framework (complex **2**) through crystallographic *c*, *b* and *a* axis respectively and structural modificantions in terms of distortion of $\{Pd(CN)_4\}^{2-}$ layers and interlayer host-host hydrogen bonding present in complex **2** at 100 K (d) and 300 K (e) respectively.

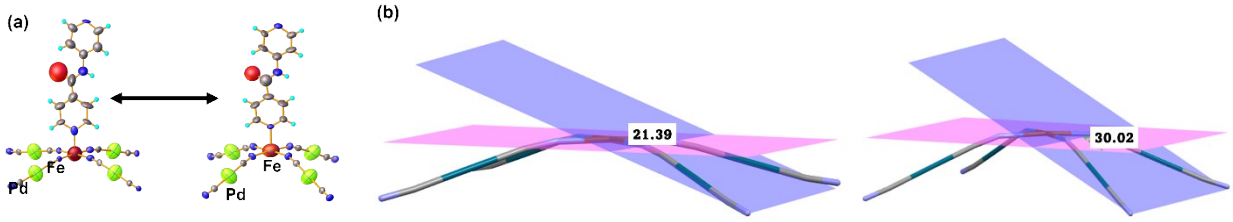

Figure S3. (a) Comparative changes around Fe center in complex **2** upon changing the temperature. Torsional angles between FeN_{eq} and $Pd(CN)_4$ planes for complex **2** at (a) 100 K and (b) 240 K.

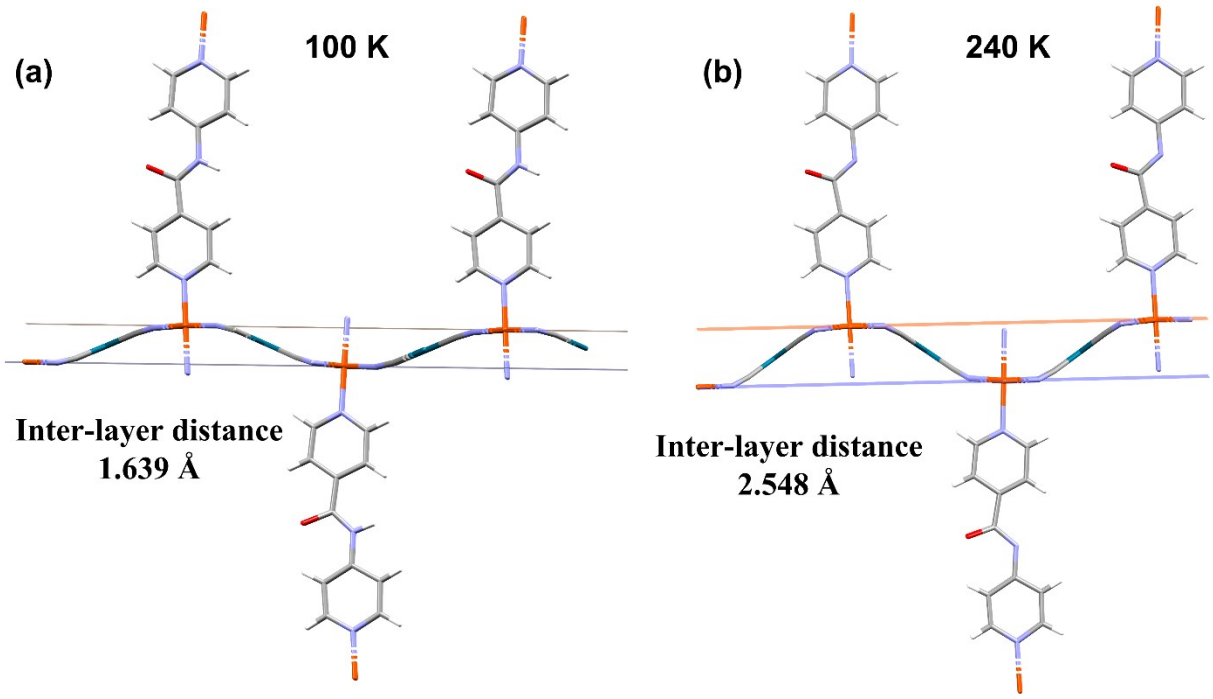

Figure S4. Comparative Fe-layer distances for complex **2** at (a) 100 K and (b) 240 K.

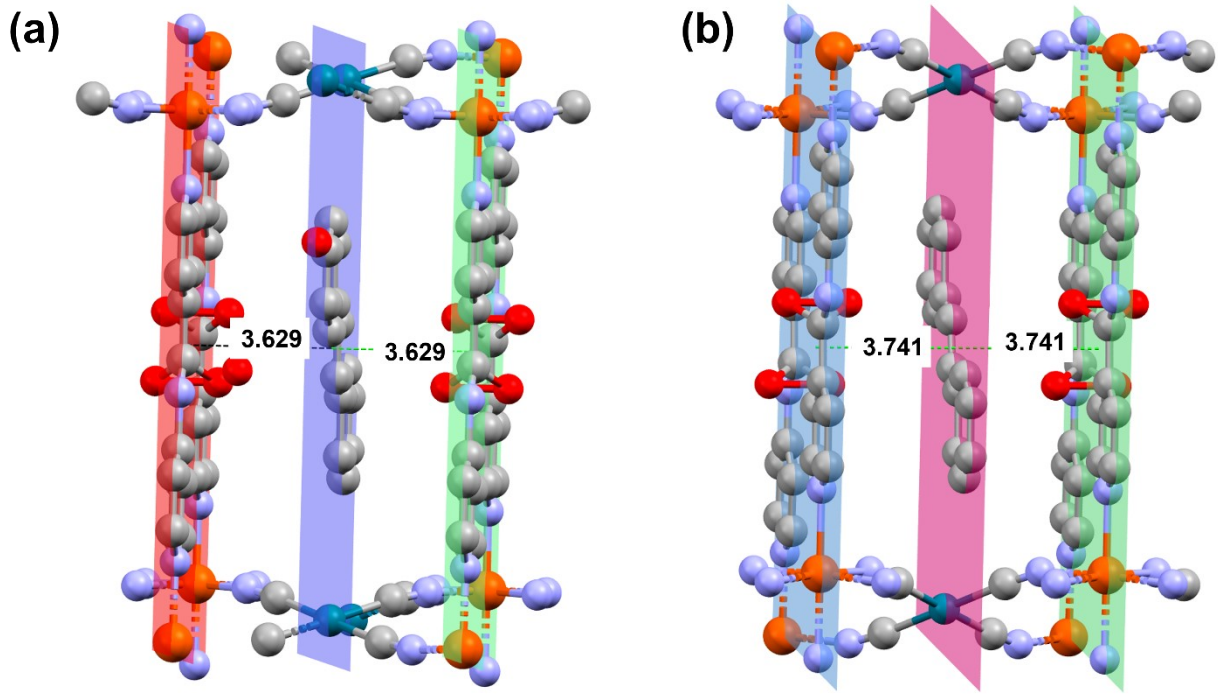

Figure S5. Comparative interplanar distance between the host and the guest of complex **2** at (a) 100 K, 3.629 Å and (b) 240 K, 3.741 Å.

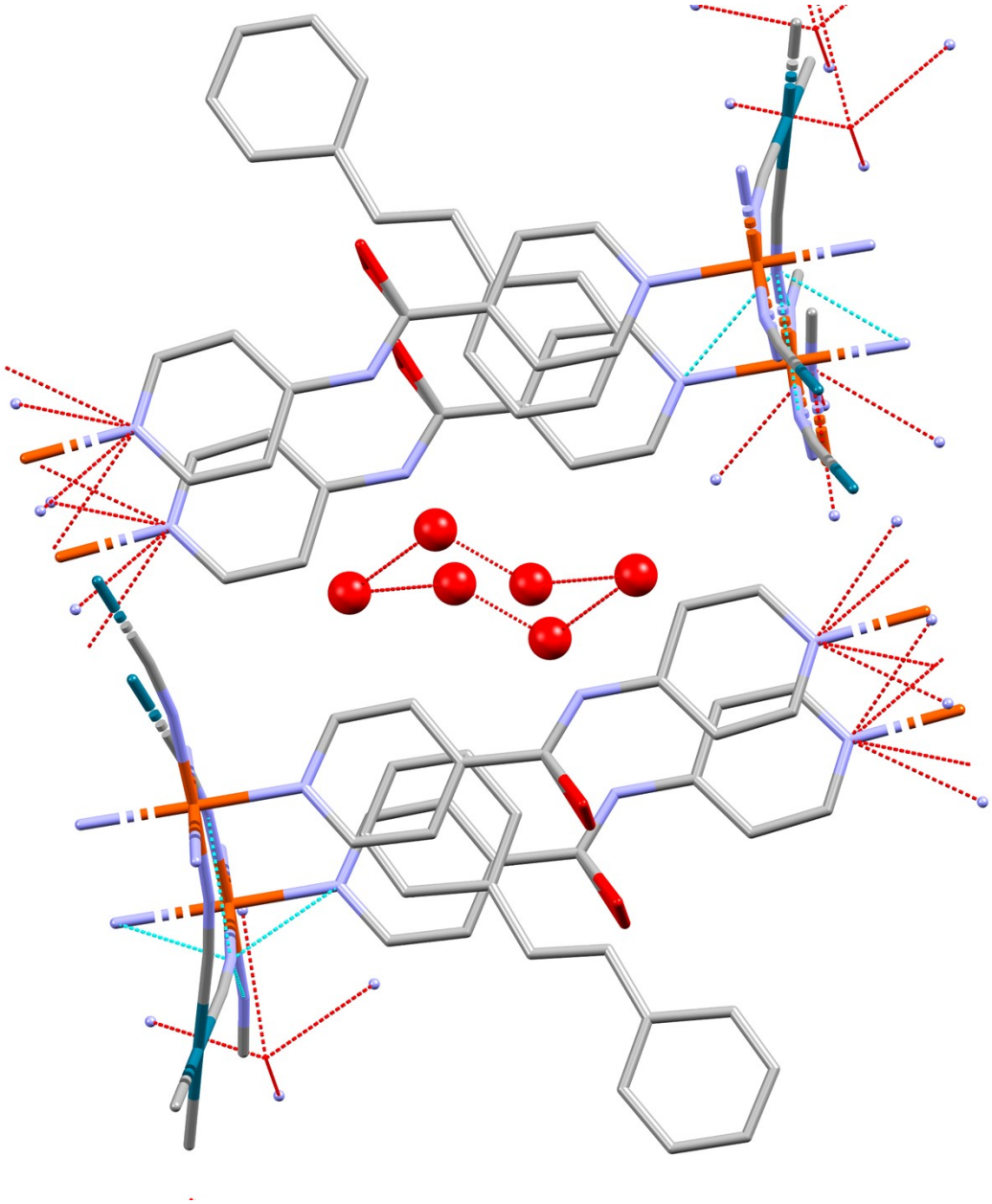

Figure S6. Cyclohexane chair-type conformation present by the residual water molecules present in the inter-layer channels of complex **2** at 100 K.

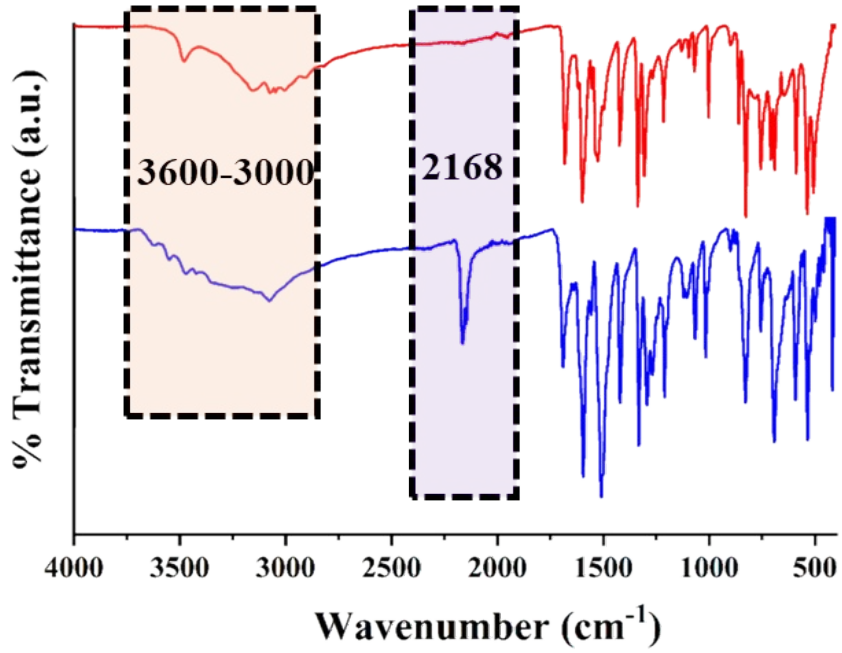

Figure S7a. FT-IR spectra of pina ligand (red) and complex **1** (blue).

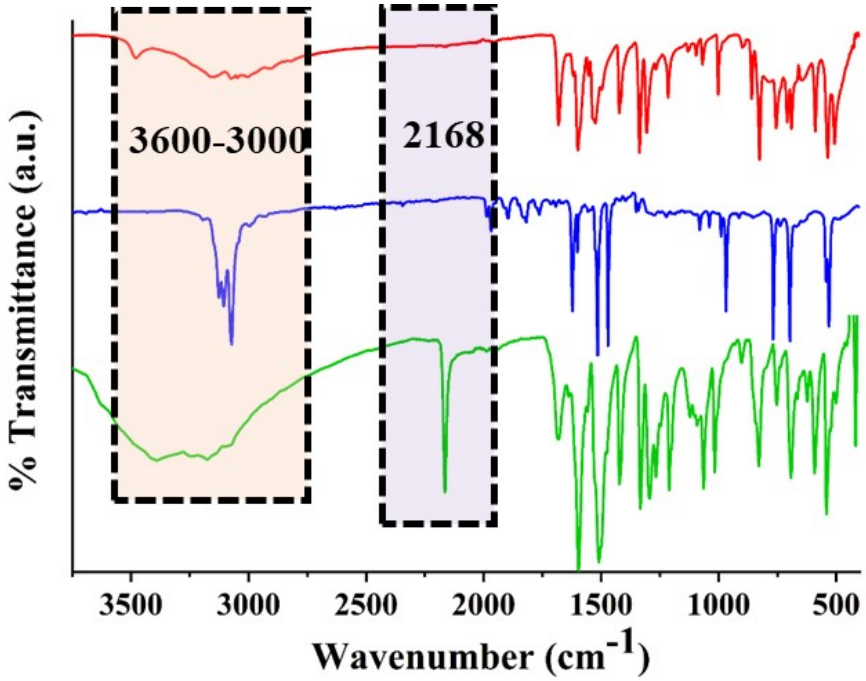

Figure S7b. FT-IR spectra of pina ligand (red), trans-stilbene(blue) and complex **2**.

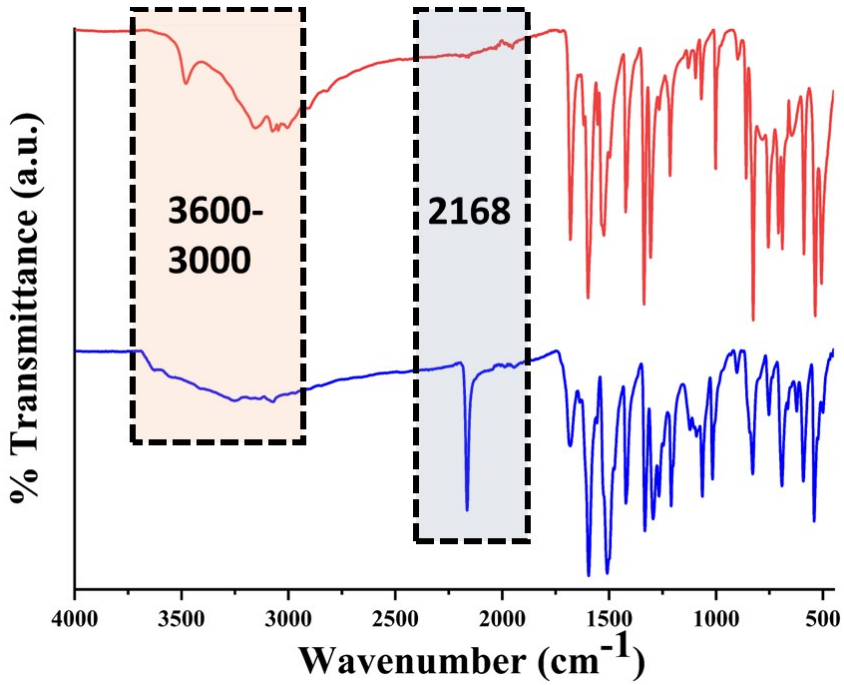

Figure S7c. FT-IR spectra of pina ligand (red) and complex 3 (blue).

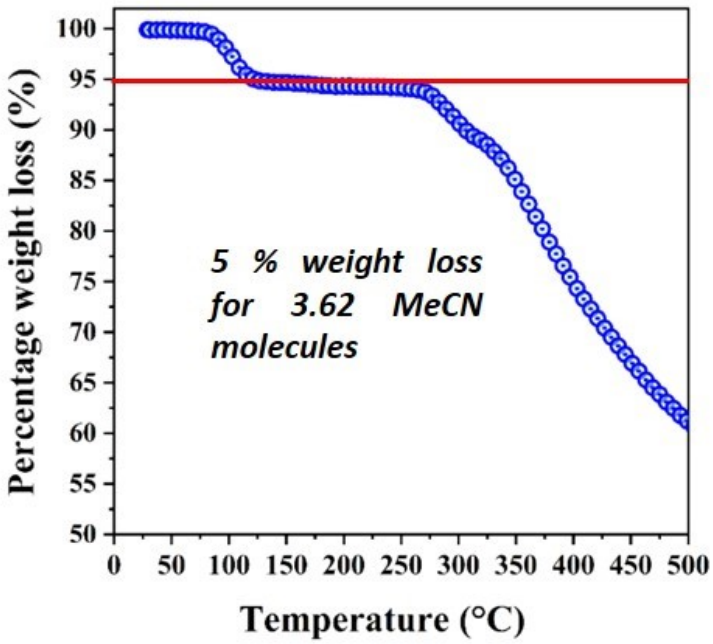

Figure S8a. TGA plot of complex **1.**

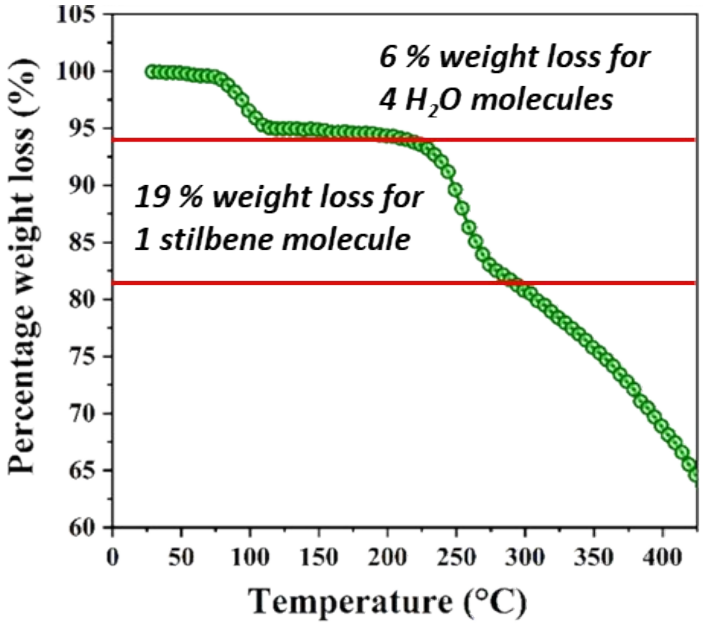

Figure S8b. TGA plot of complex **2**.

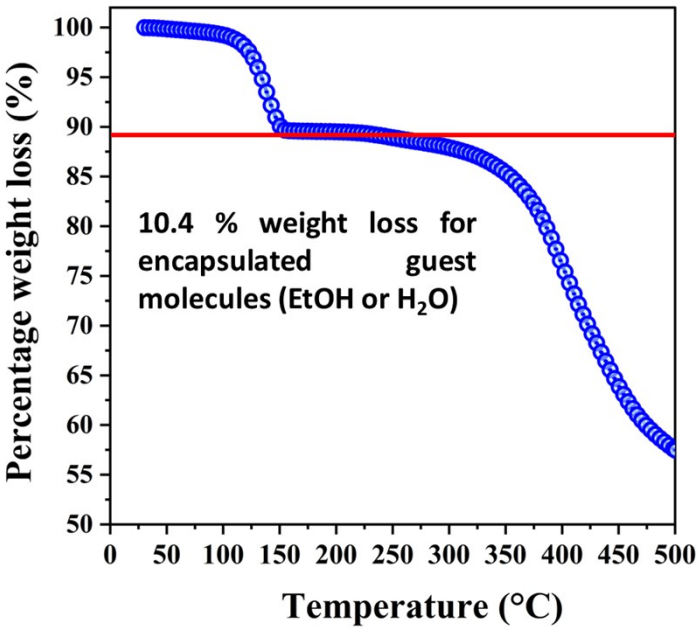

Figure S8c. TGA plot of complex 3.

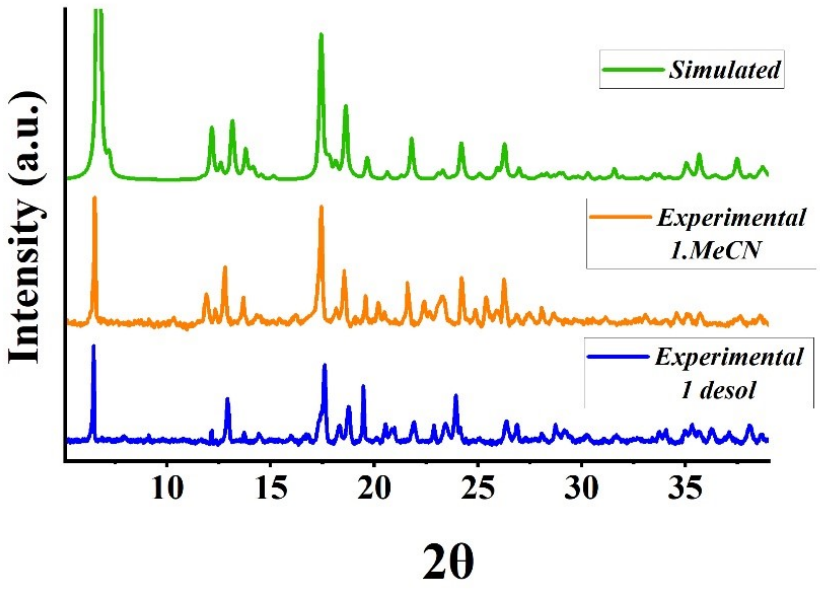

Figure S9a. PXRD plot of complex **1.**

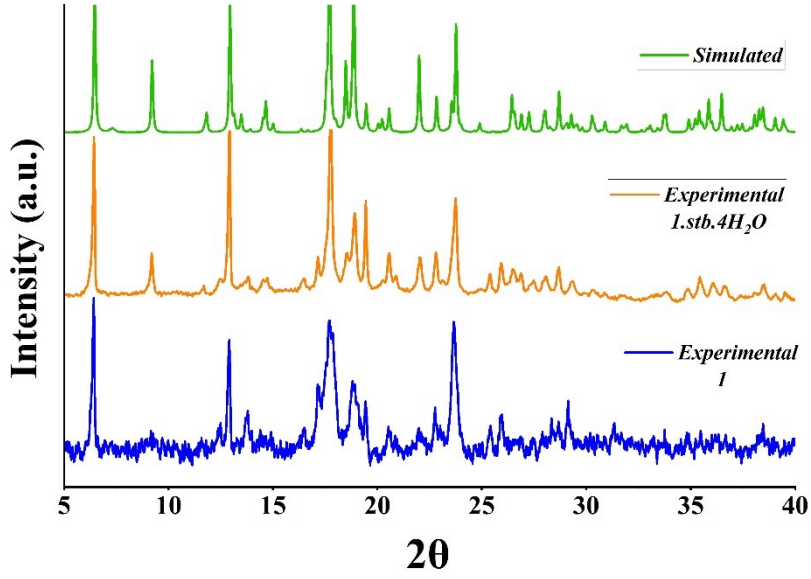

Figure S9b. PXRD plot of complex **2**.

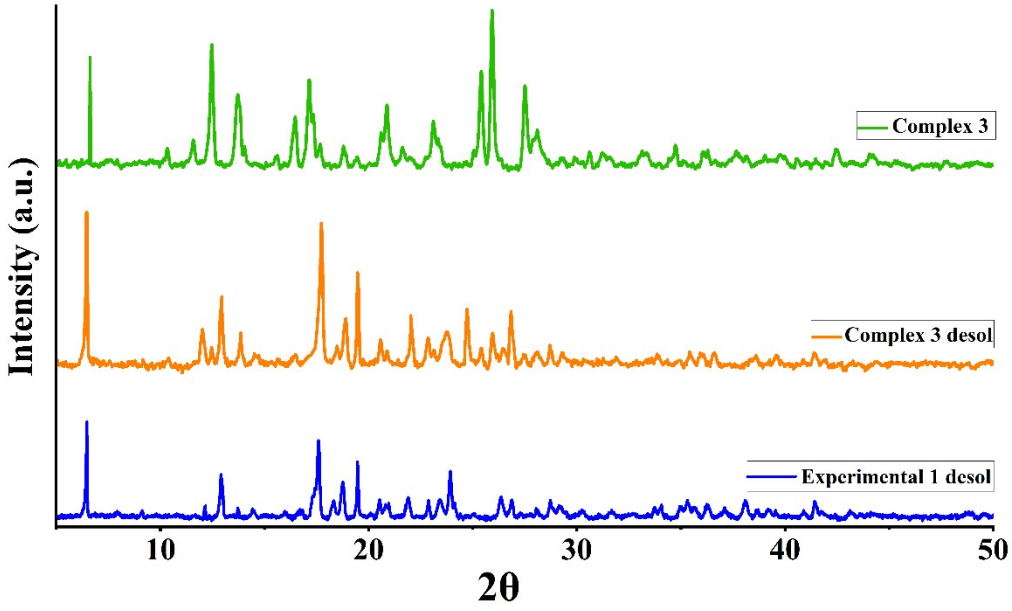

Figure S9c. PXRD plot of complex 3.

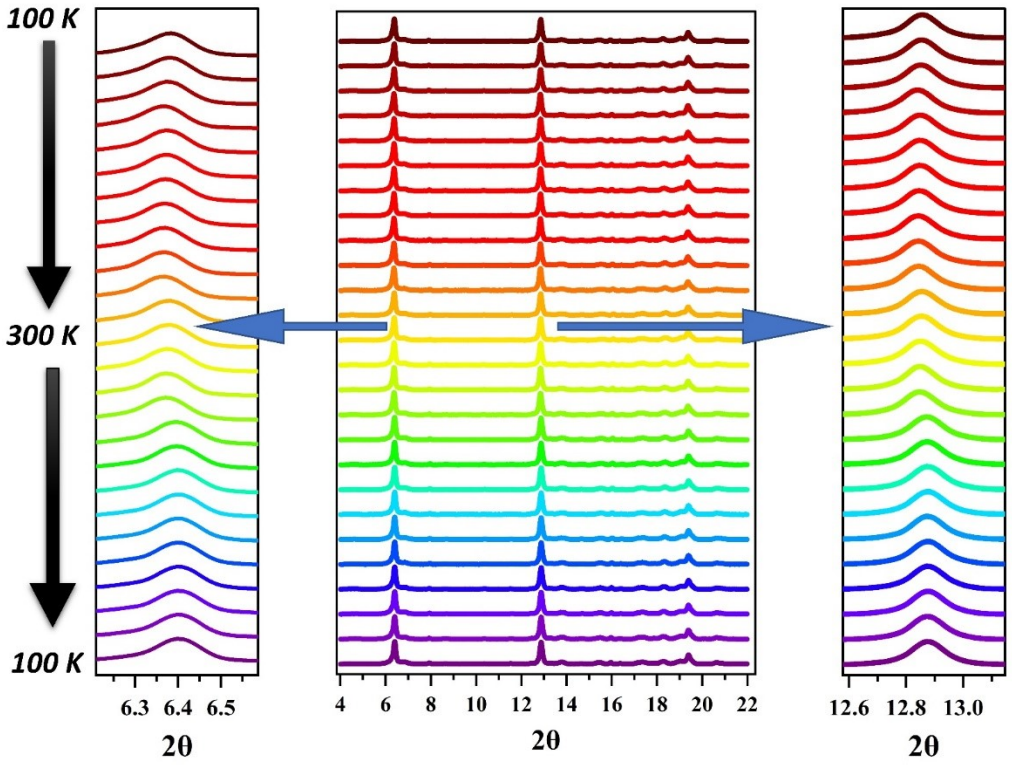

Figure S10. Variable temperature P-XRD plots of complex **2** in subsequent heating and cooling mode**.**

Magnetic Properties.

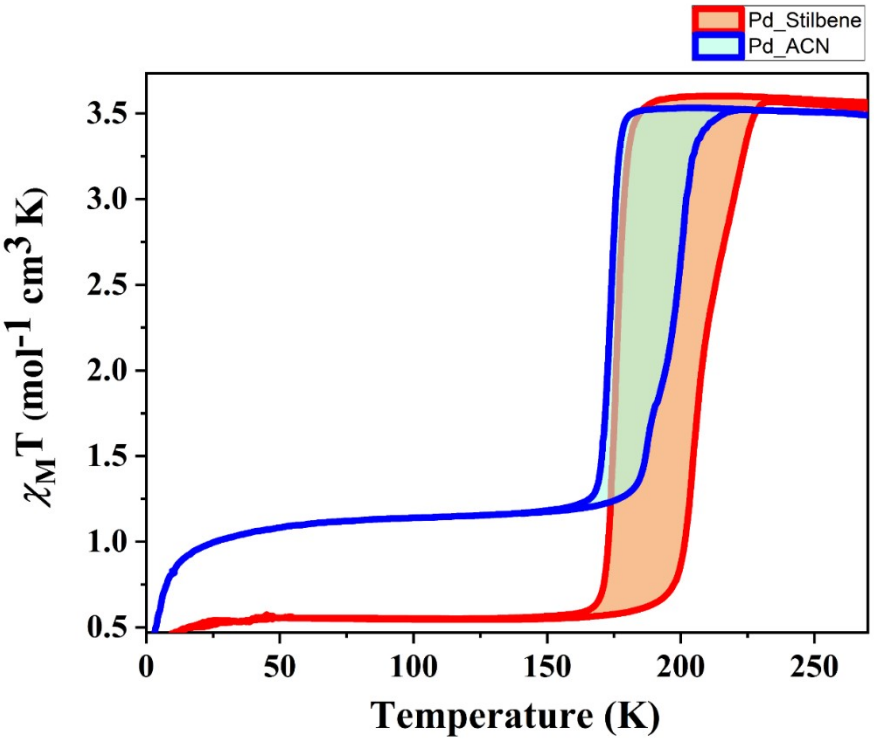

Figure S11. Variable temperature magnetic susceptibility measurements performed on polycrystalline samples of complex **1** (blue) and complex **2** (red) under the external magnetic field of 0.1 T in the temperature range of 2 to 300 K.

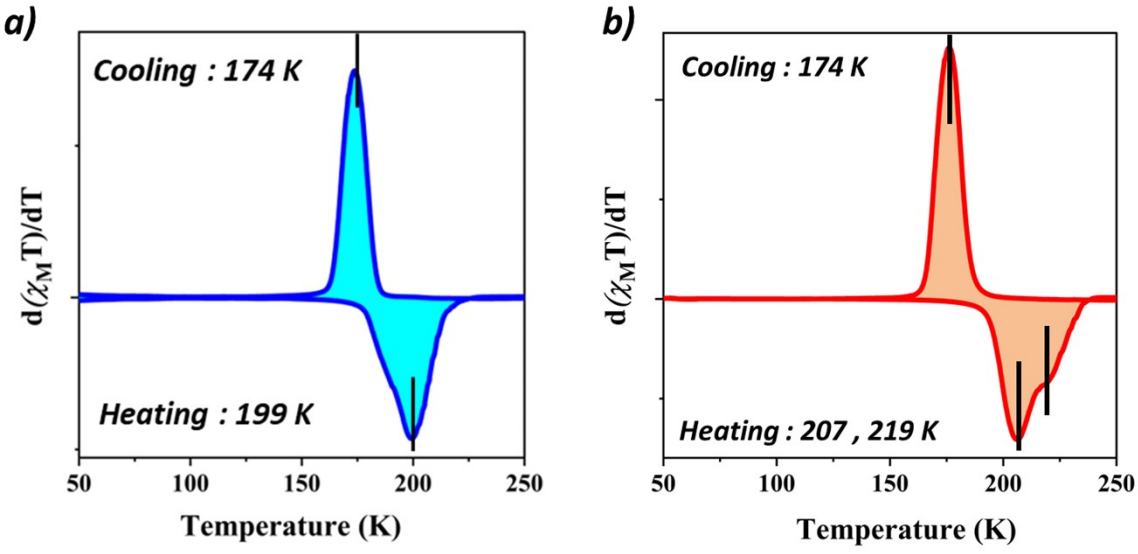

Figure S12. First derivative plot of the magnetic susceptibility data indicating the critical temperatures of transition in heating and cooling mode a) complex 1 and b) complex 2.

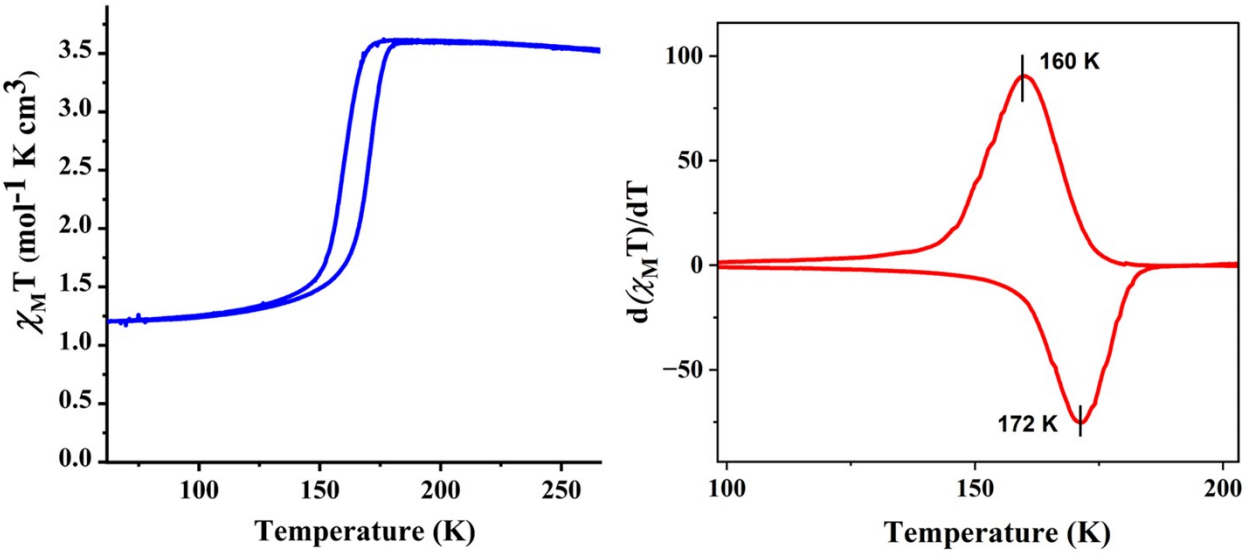

Figure S13. Magnetic susceptibility data of complex 3.

Effect of Desolvation of complex 1, complex 2 and complex 3

Complete desolvation of Complex 1 (1.3.6MeCN): To perform complete desolvatation of complex **1·3.6 MeCN,** bulk quantity of single crystals of **1·3.6 MeCN** were taken in a vial and heated at 100 °C under vacuum for an hour, according to TGA, which resulted in the guest free farmework **1**.

Partial desolvation of complex 2 (1·stb·4H_2O): Bulk quantity of single crystals of **1·stb·4H_2O** were taken in a vial and heated at 100 °C under vacuum for an hour, according to TGA to obtain the framework containing only stilbene molecules as guest (1·**stb**).

Complete desolvation of complex 2 (1·stb·4H_2O): Bulk quantity of single crystals of **1·stb·4H_2O** was taken in a vial and heated it upto 250 °C under vacuum for 3 hours, according to TGA.

Complete desolvation of Complex 3 : To perform complete desolvation of complex **3**, bulk microcrystalline powder of **3** was taken in a vial and heated at 180 °C under vacuum for an hour, according to TGA, which resulted in the guest free framework **3**.

The non-deterioration of the structural integrity after desolvation was confirmed through PXRD analyses at room temperature (Figure S9).

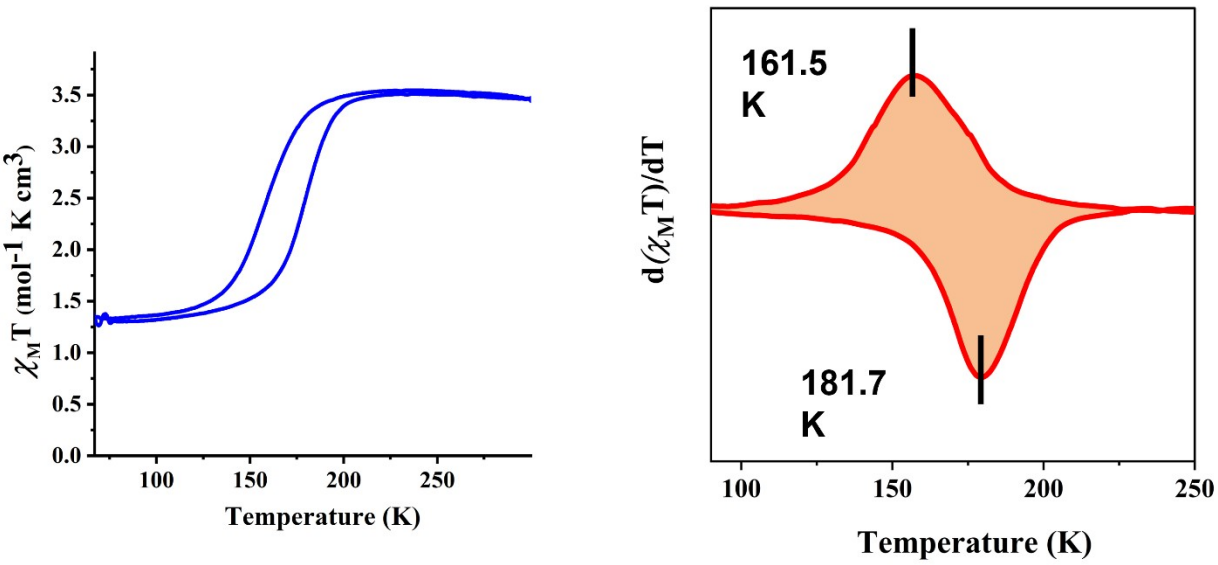

Figure S14. Magnetic susceptibility data of completely desolvated **complex 1** (i.e., framework **1**).

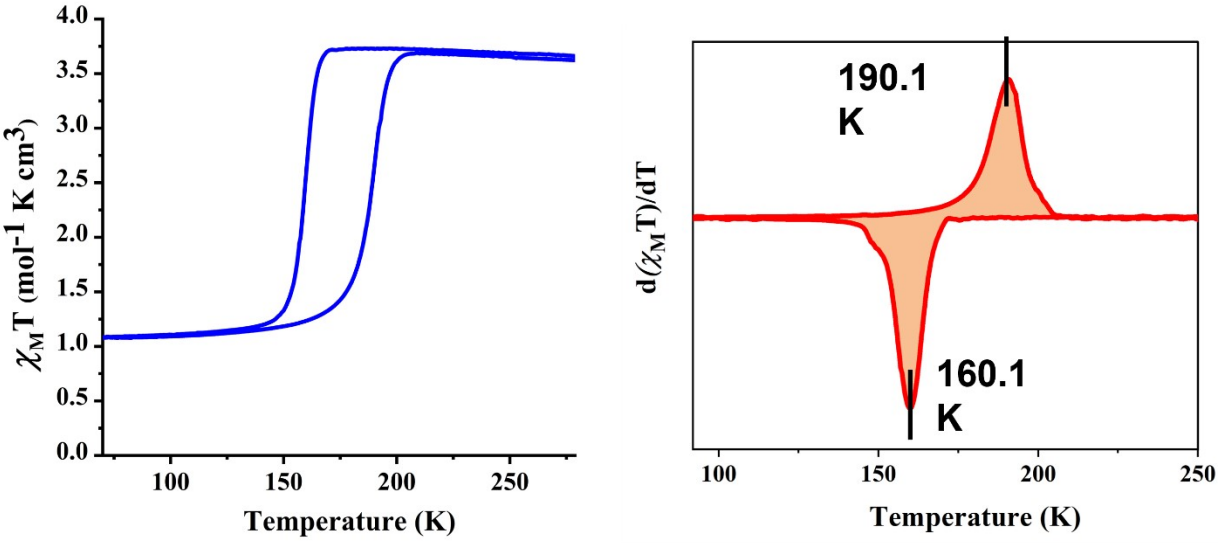

Figure. S15. Magnetic susceptibility data of Partially desolvated **Complex 2** (i.e., **1·stb**).

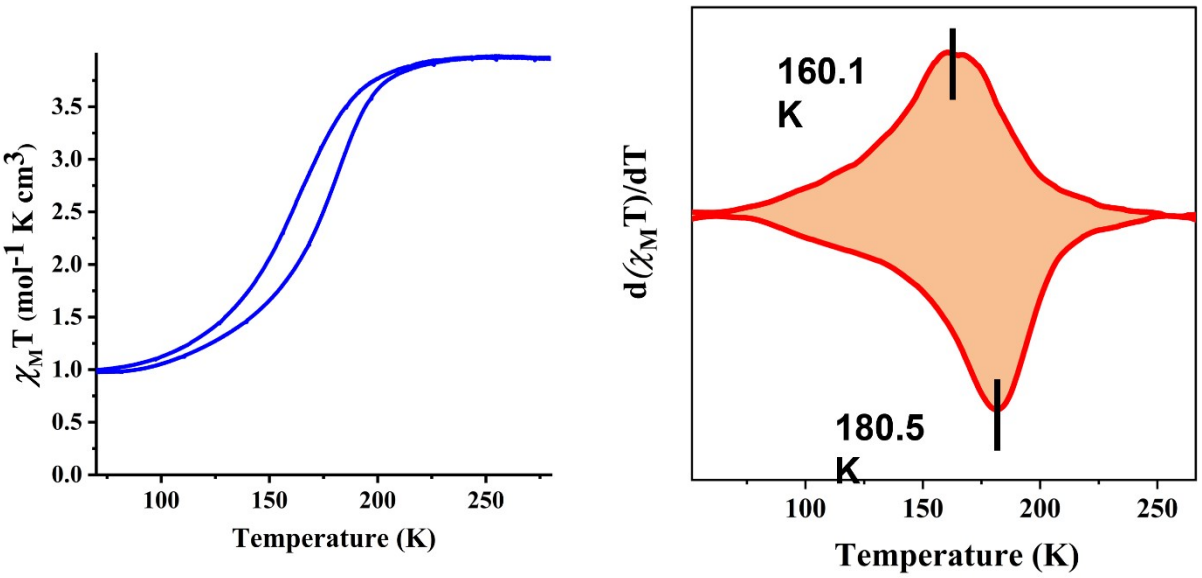

Figure S16. Magnetic susceptibility data of Completely desolvated **Complex 2** (i.e., framework **1**).

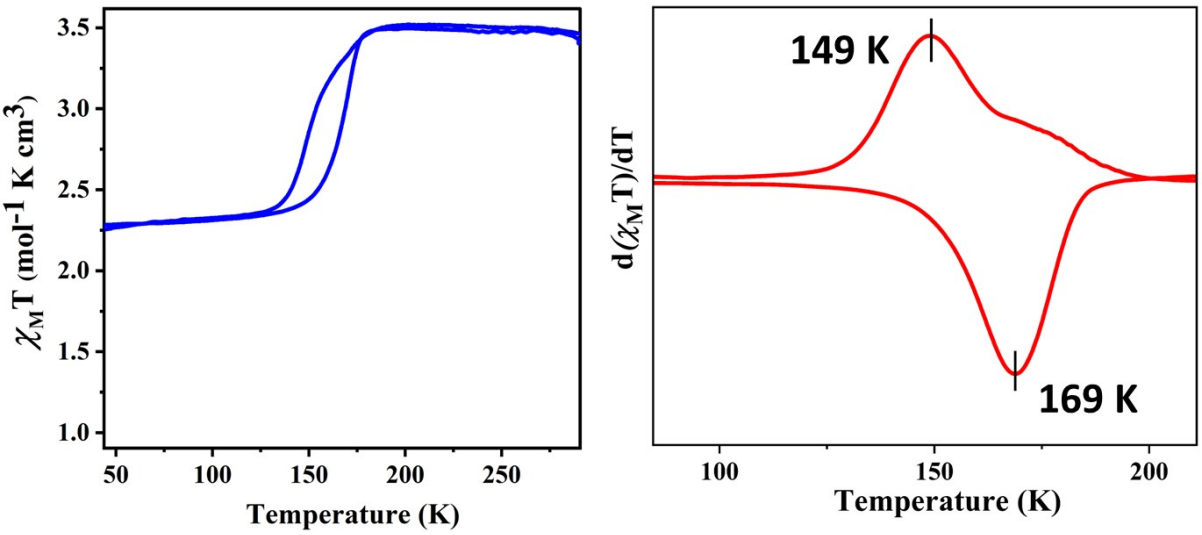

Figure S17. Magnetic susceptibility data of completely desolvated complex 3.

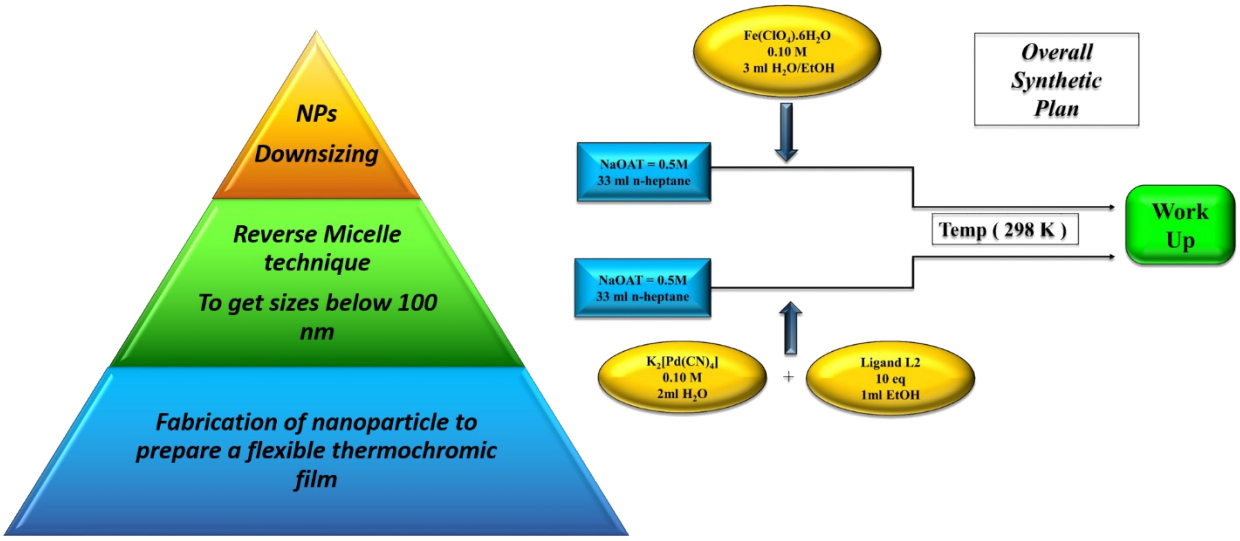

Scheme S1. Schematic representation of the nanoparticle synthesis.

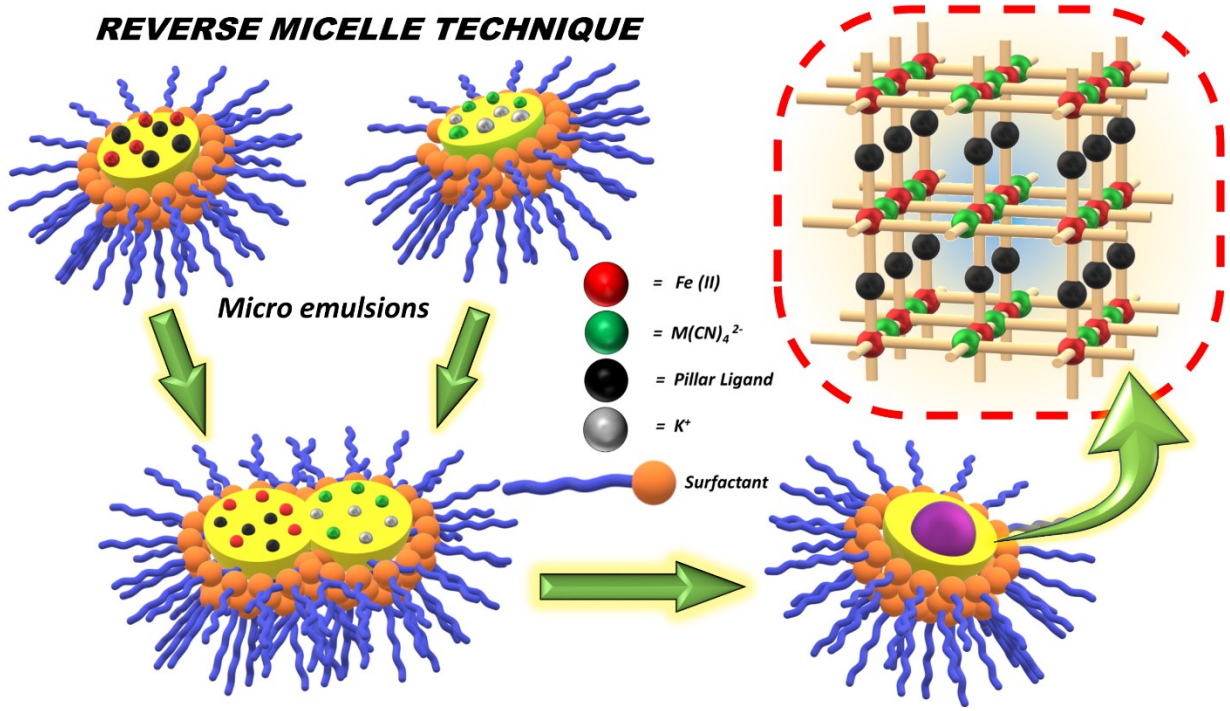

Scheme S2. Schematic diagram of reverse micelle technique used to prepare the nanoparticle.

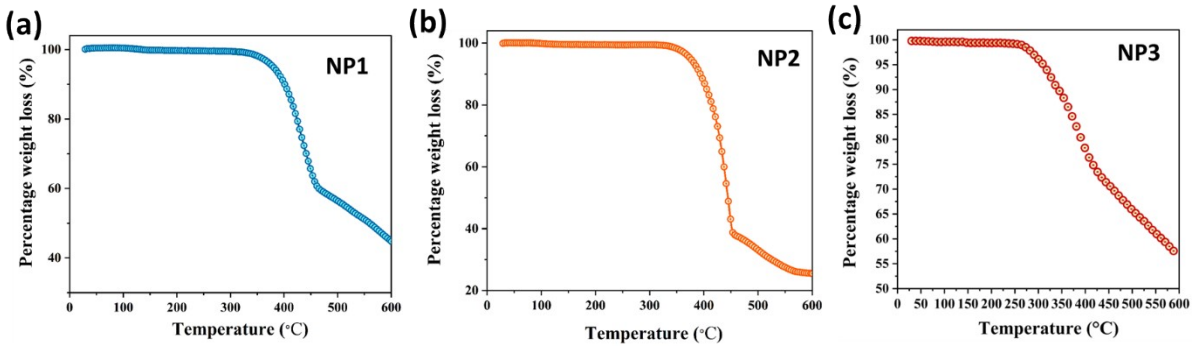

Figure S18. Thermogravimetric analyses for (a) **NP1**, (b) **NP2** and (c) **NP3**.

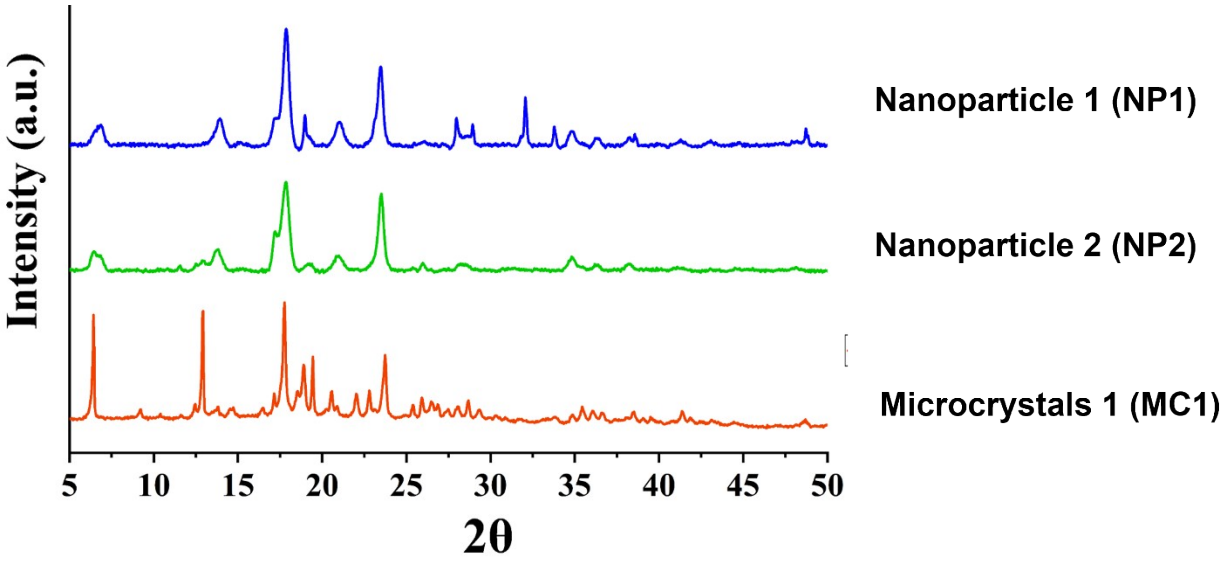

Figure S19a. Comparative PXRD analyses for the nanoparticles **NP1**, **NP2** and the bulk phase.

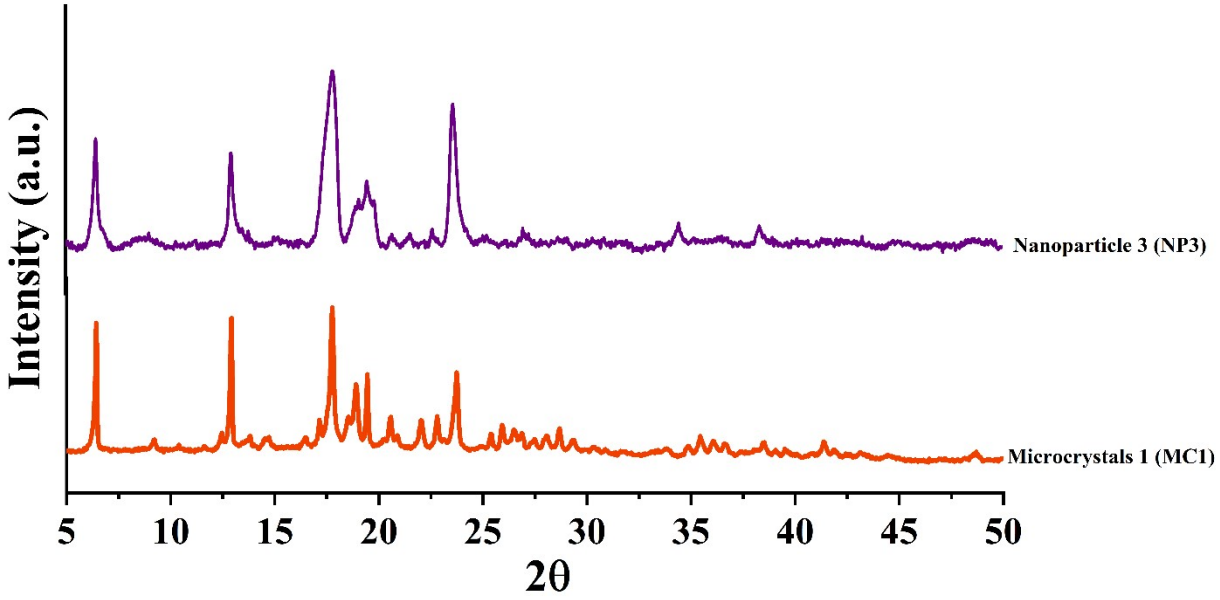

Figure S19b. Comparative PXRD analyses for the nanoparticle **NP3** and the bulk phase.

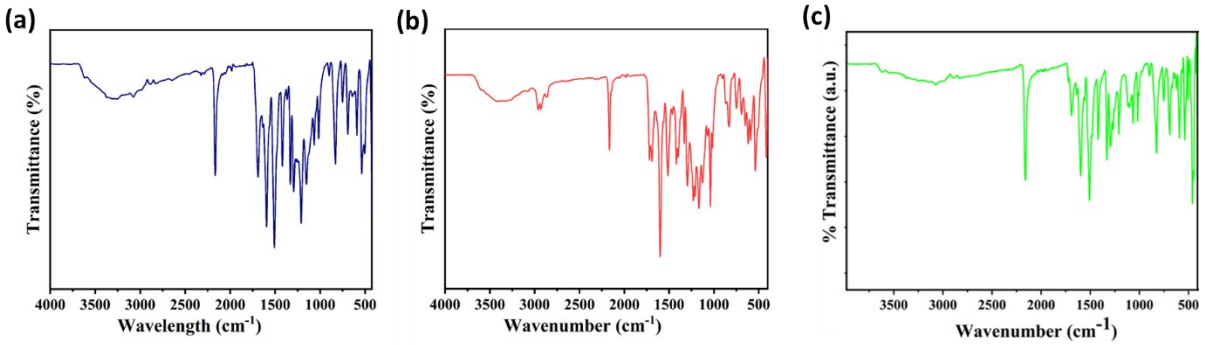

Figure S20. IR spectroscopic analyses for (a) **NP1**, (b) **NP2** and (c) **NP3**.

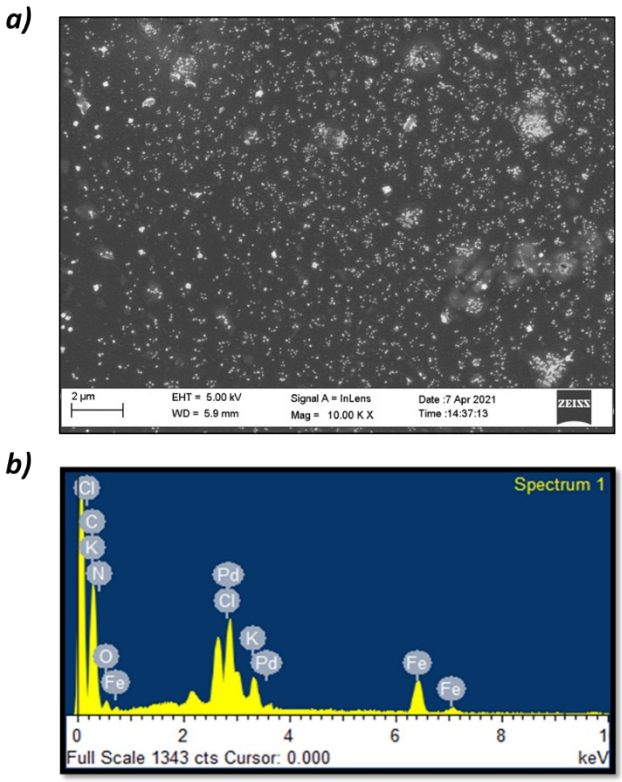

Figure S21. SEM and EDX of thermochromic film prepared by **NP1**.

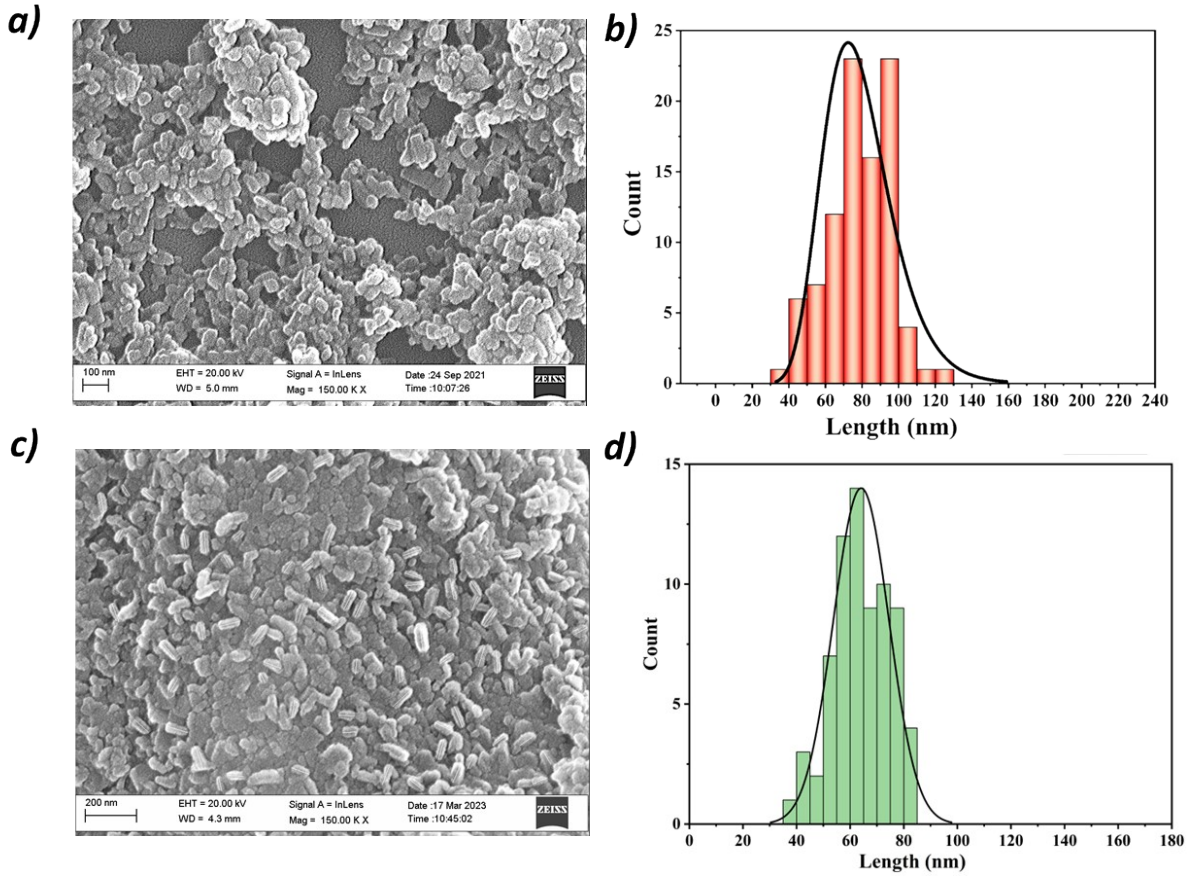

Figure S22. a) SEM image of **NP2**, b) Gaussian fitted size distribution curve of **NP2**, c) SEM image of **NP3**, d) Gaussian fitted size distribution curve of **NP3**

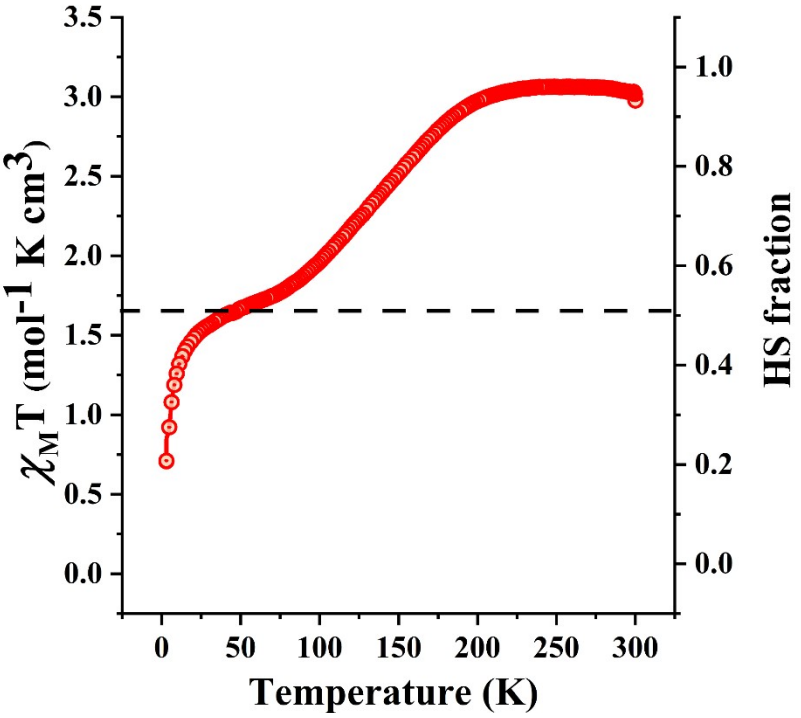

Figure S23. Magnetic plots of nanoparticle 1 (**NP1**).

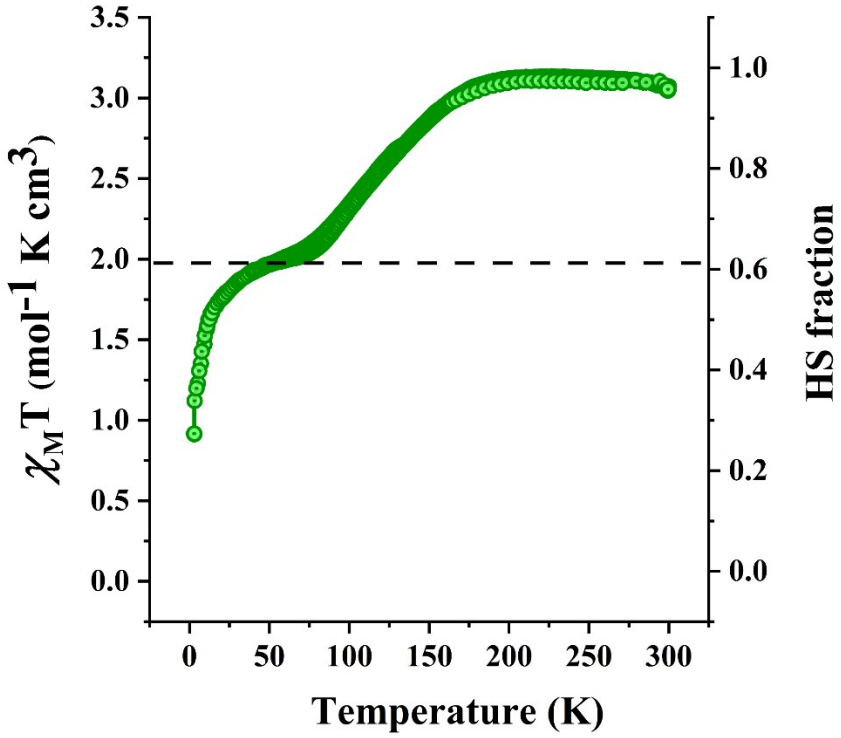

Figure S24. Magnetic plots of nanoparticle 2 (**NP2**).

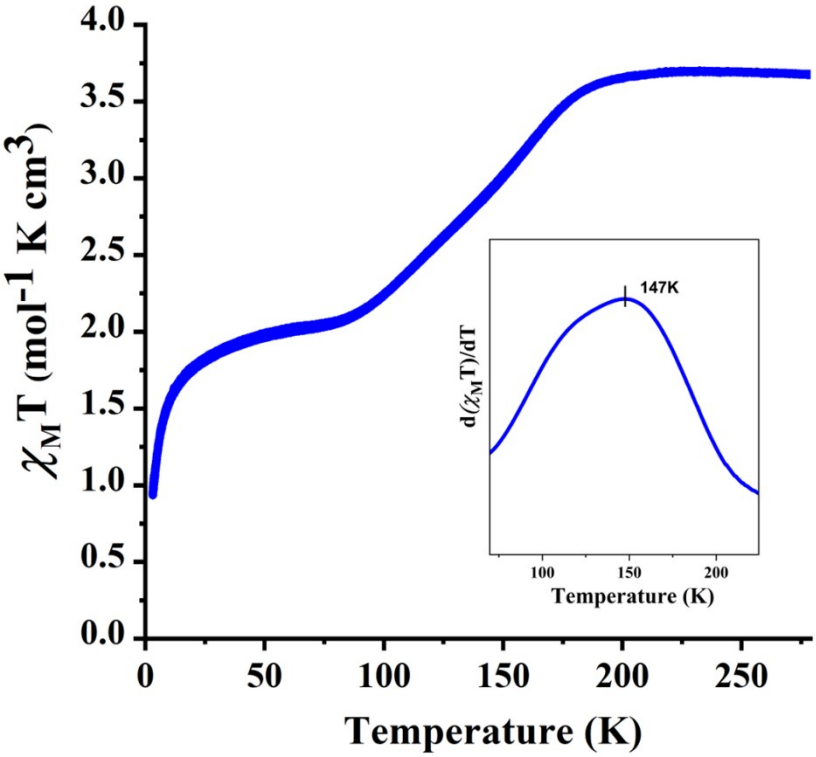

Figure S25. Magnetic plots of nanoparticle 3 (**NP3**).

Reference:-

1 O. V. Dolomanov, L. J. Bourhis, R. J. Gildea, J. A. K. Howard and H. Puschmann, *J. Appl. Crystallogr.*, 2009, **42**, 339–341.

2 G. M. Sheldrick, *Acta Crystallogr. Sect. A Found. Crystallogr.*, 2015, **71**, 3–8.

3 R. Ketkaew, Y. Tantirungrotechai, P. Harding, G. Chastanet, P. Guionneau, M. Marchivie and D. J. Harding, *Dalt. Trans.*, 2021, **50**, 1086–1096.